



## Synthesis and Electrochemical Properties of Nanocrystalline LiFePO<sub>4</sub> Obtained by Different Methods

C.G. Son<sup>a</sup>, D.R. Chang<sup>b</sup>, H.S. Kim<sup>b</sup>, and Y.S. Lee<sup>a,†</sup>

<sup>a</sup>Faculty of Applied Chemical Engineering, Chonnam National University, Gwangju 550-757, Korea

<sup>b</sup>Korea Institute of Industrial Technology, Gwangju 500-480, Korea

### ABSTRACT :

Nanocrystalline LiFePO<sub>4</sub> powders were prepared at 660-670°C in an Ar atmosphere using two different synthetic routes, solid-state and sol-gel. Both materials showed well-developed XRD patterns without any impurity peaks. Particles composed in the range of 200-300 nm from the solid-state method, and 50-100 nm from the sol-gel method, were confirmed through scanning electron microscopy and dynamic light scattering. The LiFePO<sub>4</sub> obtained by the sol-gel method offered a high discharge capacity (153 mAh/g) and stable discharge behavior, even at elevated temperatures (50 and 60°C), whereas poor electrochemical performance was observed from the solid-state method. Rate capability studies for sol gel-derived LiFePO<sub>4</sub> ranged from 0.2 to 30 C, which revealed excellent retention over 70 cycles with a 99.9% capacity.

**Keywords :** LiFePO<sub>4</sub>, Solid-state method, Sol-gel method, Cathode material, Lithium secondary battery

Received May 10, 2011 : Accepted June 29, 2011

### 1. Introduction

In the recent past, researchers have focused upon a group of lithium iron-containing compounds that incorporate polyanions of the class XO<sub>4</sub><sup>3-</sup> (X = S, P, As, Mo).<sup>1-5</sup> Among them, LiMPO<sub>4</sub> (where M = Fe, Mn, Co, Ni) groups proved very attractive. The search for lithium metal phosphates as potential cathode materials for lithium secondary batteries is paramount given their low cost, low toxicity, excellent thermal stability, and environmental aspects when compared to the existing commercialized LiCoO<sub>2</sub>.<sup>1,3</sup> In particular, due to their unique properties, they are very suitable for large-scale lithium batteries in applications related to electric vehicles (EVs), plug-in hybrid electric vehicles (PHEVs), and stationary storage batteries.

Such large polyanions (PO<sub>4</sub><sup>3-</sup>) from the olivine group can stabilize structure through strong P-O covalent

bonding and tune the M<sup>3+</sup>/M<sup>2+</sup> redox potential to a useful level *via* the M-P-O inductive effect.<sup>5</sup> Among them, LiFePO<sub>4</sub> was first proposed by Padhi *et al.*<sup>1</sup>) and has generated much interest over the last decade in the search for desirable cathode materials for the next generation of lithium secondary batteries. LiFePO<sub>4</sub> shows a redox potential near 3.45 versus Li<sup>+</sup>/Li, with a high theoretical capacity (170 mAh/g), when compared to the proposed alternate cathode materials for LiCoO<sub>2</sub>. However, LiFePO<sub>4</sub> suffers interims of inherent electronic conductivity and poor rate capability, which hinders full-capacity utilization. In order to circumvent these issues, several approaches have been adopted, particularly, controlling grain size, which improves Li<sup>+</sup> ion diffusion *via* shortening the path length,<sup>6</sup> conducting surface coatings such as carbon,<sup>7-12</sup> and metal doping of the Fe sites,<sup>1, 13</sup> all of which improve LiFePO<sub>4</sub> electrochemical performance. Moreover, the synthetic routes include important phenomena in order to achieve the desirable properties. Several methods have thus been proposed to prepare LiFePO<sub>4</sub>, such as solid-state,<sup>14</sup> co-precipitation,<sup>15</sup> hydrothermal,<sup>16,17</sup>

<sup>†</sup>Corresponding author. Tel.: +82-62-530-1904

E-mail address: leeys@chonnam.ac.kr

and sol-gel methods.<sup>18-20)</sup> Among the procedures, the solid-state method has proved very useful and appealing for mass production on an industrial scale. However, it is not without several disadvantages, such as inhomogeneity, irregular morphology, and larger particle sizes with a broader particle size distribution. While the sol-gel process possesses many advantages, including good stoichiometric control and production of submicron sized particles with a narrow particle size distribution, its synthesis is complex and costly.

In the present paper, we compare two types of synthetic methods, solid-state and sol-gel, which yielded various physico-chemical and electrochemical properties of the final  $\text{LiFePO}_4$  powders. We also confirm the importance of determining the optimum synthetic method and conditions for the  $\text{LiFePO}_4$  electrode material to give excellent battery performance in the  $\text{Li}/\text{LiFePO}_4$  system.

## 2. Experimental

The nanocrystalline  $\text{LiFePO}_4$  was synthesized from  $\text{Li}_2\text{CO}_3$ ,  $\text{Li}(\text{CH}_3\text{COO})$  (Sigma-Aldrich, USA),  $\text{FeC}_2\text{O}_4 \cdot 2\text{H}_2\text{O}$ ,  $\text{Fe}(\text{CH}_3\text{COO})_2$  (Aldrich, USA),  $(\text{NH}_4)_2\text{HPO}_4$  (Sigma-Aldrich, USA), and  $\text{C}_6\text{H}_{10}\text{O}_4$  (Sigma-Aldrich, USA), using either the solid-state (SS) or sol-gel (SG) methods. The detailed synthetic procedures and conditions are described graphically in Fig. 1. In brief, for the SS method, a stoichiometric amount of each material was ground and calcined at  $400^\circ\text{C}$  for 1.5 h and then again fine ground and fired at  $660^\circ\text{C}$  for 2.5 h in an Ar atmosphere using a tubular furnace. For the SG method, adipic acid was chosen as a chelating agent to prevent agglomeration of the particles during the synthesis. A stoichiometric amount of each material was dissolved in ethanol and thoroughly mixed in an aqueous solution of adipic acid using magnetic stirring and heating. The solution

was evaporated at  $90^\circ\text{C}$  for 4 h to form a transparent gel. Then, the gel was transferred into a vacuum oven to generate the precursors. The precursor was initially calcined at  $400^\circ\text{C}$  for 3 h in Ar and the resulting product again grounded using a mortar, and again placed at  $670^\circ\text{C}$  for 5 h under an Ar flow.

Powder X-ray diffraction analyses (CuK $\alpha$  radiation) were performed (XRD, Rint 1000, Rigaku, Japan) to determine the crystalline phase of the prepared materials. Particle size distributions were determined using a dynamic light scattering system (DLS-7000(AL), Otsuka electronics, Japan). Particulate morphologies were observed using a field emission scanning electron microscope (FE-SEM, S-4700, Hitachi, Japan). Inductively coupled plasma (ICP)-atomic emission spectrometry (Optima 4300 DV, Perkin-Elmer, USA) was used to study  $\text{Fe}^{2+}$  dissolution in the electrolytes. Electrochemical characterizations were performed using a CR2032 coin-type cell. The cathode was fabricated with 20 mg of precisely weighed active material, 3 mg of Ketzen black, and 3 mg of conductive binder (2 mg of Teflonized acetylene black (TAB) and 1 mg of graphite). It was pressed on a  $200\text{-mm}^2$  stainless steel mesh, which acted as a current collector for the cathodes, under a pressure of  $300\text{ kg/cm}^2$ , and dried at  $130^\circ\text{C}$  for 5 h in a vacuum oven. The test cell was made up of a cathode and a lithium metal anode separated by a porous polypropylene film (Celgard 3401). A mixture of 1.0 M  $\text{LiPF}_6$  in ethylene carbonate (EC)/dimethyl carbonate (DMC) (1 : 1 vol. with  $< 3.3\text{ ppm H}_2\text{O}$ , Techno Semichem, Korea) was used as the electrolyte. A current density of  $0.1\text{ mA/cm}^2$  was fixed for the charge-discharge process with a potential window between 2.8 to 4.0 V at room temperature, as well as elevated temperatures ( $50$  and  $60^\circ\text{C}$ ). The rate capability studies were also performed at room temperature with various current densities from 0.1 C-30 C.

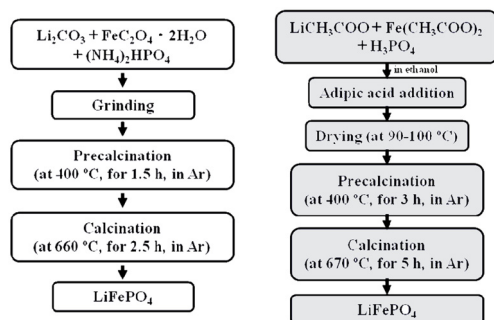


Fig. 1. Pictorial representation of synthetic procedures.

## 3. Results and Discussion

Fig. 2 shows the X-ray diffraction (XRD) patterns of the  $\text{LiFePO}_4$  materials obtained by the SS and SG methods. The XRD results clearly show  $\text{LiFePO}_4$  with a well-ordered olivine structure indexed to the  $Pnma$  space group and without any impurities such as  $\text{FeP}$ ,  $\text{Fe}_2\text{P}$ , and  $\text{Li}_3\text{PO}_4$ .<sup>19)</sup> The exact compositions of the prepared materials were  $\text{Li}_{0.99}\text{FePO}_{4.01}$  for SS and  $\text{LiFePO}_{4.01}$  for SG, confirmed by Rietveld refinement (not shown). The lattice constants of the  $\text{LiFePO}_4$  material obtained were :  $a = 10.341\text{ \AA}$ ;  $b = 6.010\text{ \AA}$ ;  $c = 4.698\text{ \AA}$  for SS, and

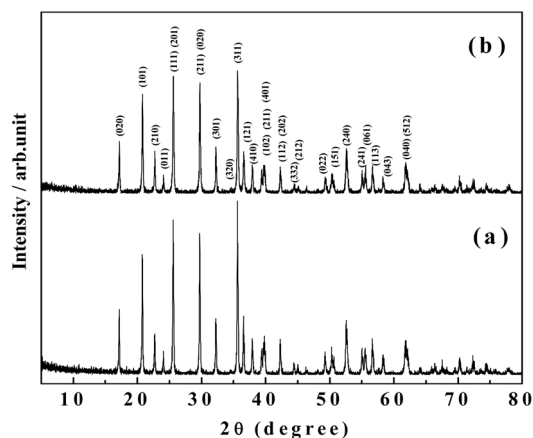


Fig. 2. XRD patterns of  $\text{LiFePO}_4$  synthesized by (a) solid-state method and (b) sol-gel method.

$a = 10.343 \text{ \AA}$ ;  $b = 6.012 \text{ \AA}$ ;  $c = 4.697 \text{ \AA}$  for SG, respectively; these values were similar to previous reports.<sup>22)</sup>

Fig. 3 presents the SEM micrographs of the nanocrystalline  $\text{LiFePO}_4$  powders obtained by different procedures. The images clearly show the appearance of polycrystalline particles, in addition to select small particles. The  $\text{LiFePO}_4$  material obtained by the SG route was composed of small particles ranging between 50-100 nm, when compared to the SS route (200-400 nm). The small particles possess a high surface area; this is one prerequisite for accommodating large levels of  $\text{Li}^+$  ions during the cycling process, which reveal good electrochemical performance of the cell.<sup>16-18)</sup>

The exact size of the prepared particles by the different methods were calculated by dynamic light scattering (DLS) and presented in Fig. 4. The majority of the particles lies between 200 to 400 nm for the SS route, whereas  $< 100 \text{ nm}$  was observed for the SG method. Generally, with a solution-based synthesis process such as SG route, the

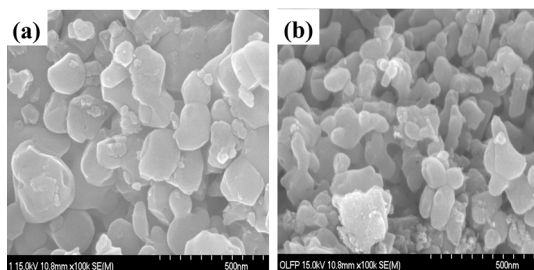


Fig. 3. FE-SEM images of  $\text{LiFePO}_4$  obtained by (a) solid-state method and (b) sol-gel method.

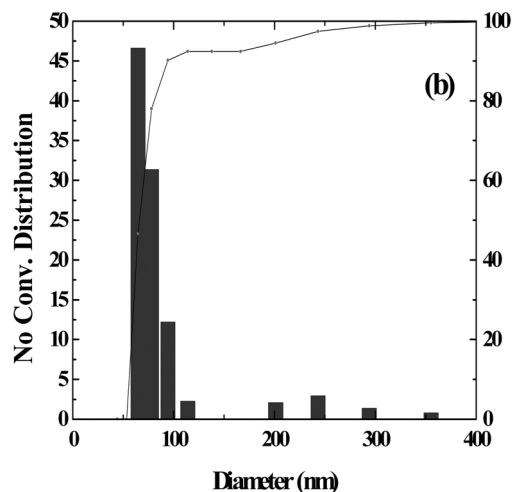
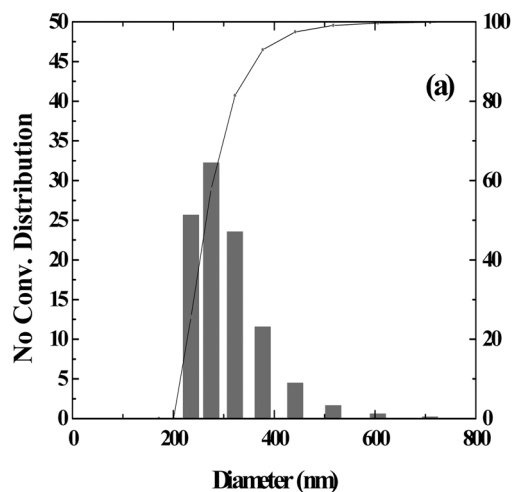


Fig. 4. Particle size distribution of  $\text{LiFePO}_4$  obtained by (a) solid-state method and (b) sol-gel method.

particle size can be effectively controlled introduction of a chelating agent. Nevertheless, in this case, oxidation of iron is much easier than in the solid phase.<sup>23)</sup> Thus, in order to prevent such oxidation, a chelating agent (adipic acid) is necessary during preparation of the precursor gel. Furthermore, chelating agents also hinder particle growth during the calcination process, resulting in a reduced grain size in the resultant material.<sup>24)</sup> The DLS measurement results highly parallel the appearance of particles from the SEM observations.

Fig. 5 illustrates the typical initial charge and discharge curves of  $\text{Li}/\text{LiFePO}_4$  cells with a current density of  $0.1 \text{ mA/cm}^2$  between 4.0-2.8 V at ambient

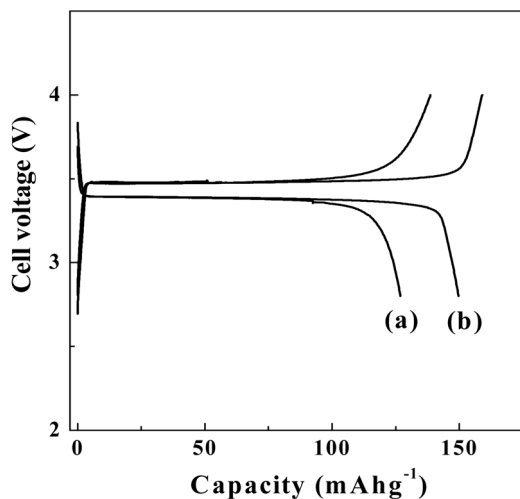


Fig. 5. The first charge/discharge curves of the Li/LiFePO<sub>4</sub> cell prepared by (a) solid-state method and (b) sol-gel method.

temperature. Both the Li/LiFePO<sub>4</sub> cells exhibited typical electrochemical behavior with a long distinct voltage plateau near 3.45 V in the first charge, indicating a phase transition of triphylite LiFePO<sub>4</sub> to heterosite FePO<sub>4</sub>. The LiFePO<sub>4</sub> obtained from the SG route delivered a high initial discharge capacity of 149 mAh/g, while LiFePO<sub>4</sub> from the SS route exhibited a capacity of 126 mAh/g. The high discharge capacity may be due to the presence of a chelating agent (adipic acid). During the calcination process, the chelating agent is converted into amorphous carbon and effectively coated onto the surface of the active particles.<sup>5)</sup> There are many advantages of using a chelating agent: (i) effective control of the particle growth to provide high surface area nanoparticles, which leads to accommodation of large amounts of Li<sup>+</sup> ions;<sup>24)</sup> (ii) reduced grains reveal faster kinetics for Li<sup>+</sup> ions *via* reducing path length; (iii) enhanced electronic conductivity through surface coating of carbon, which is derived from carbonization of the chelating agent; (iv) prevention of unwanted side reaction with electrolytes through the protective coating of carbon.<sup>25)</sup>

Fig. 6 shows the room temperature cycling performance of the Li/LiFePO<sub>4</sub> cells by different methods. As expected, the SG-derived cell showed an excellent cycle performance over 50 cycles. The increasing capacity trend was observed for up to the 3rd cycle, beyond which, it exhibited a perfect cycle performance without any capacity fade (153 mAh/g). The cell experienced a coulombic efficiency of > 99.9% for the 50 observed cycles. Though

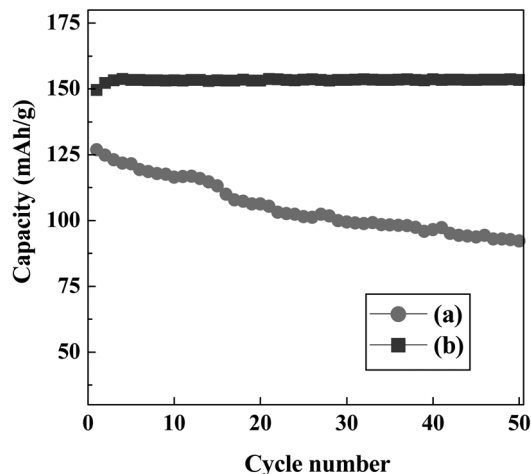


Fig. 6. Room temperature cycling performance of the Li/LiFePO<sub>4</sub> cells prepared by (a) solid-state method and (b) sol-gel method.

this cell demonstrated excellent cycling performance, the discharge capacity was slightly lower than the theoretical value. Conversely, the SS-derived cell experienced a continuous capacity fade during the cycling, with a reduced capacity relative to the SG-derived LiFePO<sub>4</sub>. The continuous capacity fade arose due to the sluggish Li<sup>+</sup> ion diffusion kinetics routed through the poor electronic conductivity and dissolution of the Fe<sup>2+</sup> ion from the active material in the electrolyte solution, which is possible due to the presence of HF. The presence of the dangerous HF in all LiPF<sub>6</sub>-based electrolytes is unavoidable. Furthermore, HF content increases due to the hydrolysis of LiPF<sub>6</sub> against the trace amount of moisture present in the atmosphere.<sup>26-28)</sup> The increasing HF content provides poor cycling performance of the cell due toward dissolution of the cations.<sup>27)</sup>

The elevated temperature (50 and 60°C) performances of the cells were demonstrated and given in Fig. 7. At 50 and 60°C, the SS-derived LiFePO<sub>4</sub> material exhibited behavior similar to the room temperature profile. However, at elevated temperature conditions, the SG-derived LiFePO<sub>4</sub> materials exhibited a stable and perfect discharge behavior. A negligible amount of capacity fade was observed at 60°C. This type of stability may be attributed to the protective coating of the chelating agent in the form of carbon on the active material surface. This adversely prevents the side reaction with the electrolyte counterparts, especially HF.<sup>29-31)</sup>

From the above studies, the SG synthesis of LiFePO<sub>4</sub>

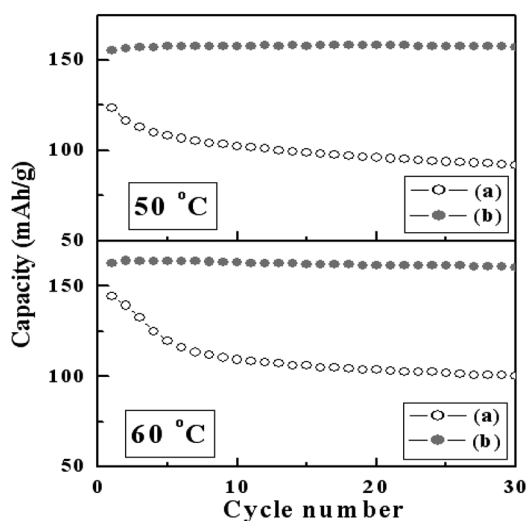


Fig. 7. Elevated temperature cycling performance of the Li/LiFePO<sub>4</sub> cells prepared by (a) solid-state method and (b) sol-gel method.

demonstrated excellent cycling performance, even at elevated temperature conditions. Further, in order to ascertain the high rate capability of the cell, the LiFePO<sub>4</sub> obtained from the SG route was subjected to different current densities ranging from 0.1 to 30 C, at ambient temperature (Fig. 8). The cell delivered 162 mAh/g at 0.2 C, with the discharge capacity decreasing with an increasing current rate. At 30 C, the cell exhibited a discharge capacity over 58 mAh/g; this value was one of the better results obtained through the SG process when compared to other reports by Wang *et al.*<sup>18)</sup> and Choi and Kumta.<sup>32)</sup> In addition, this study was repeated as a function of cycle to ensure the capacity retention of the material prepared. The same results were observed for subsequent testing with 99.9% retention.

To better understand the poor electrochemical properties of the LiFePO<sub>4</sub> obtained from the SS route, the material was subjected to aging tests in the presence of an electrolyte solution (1.0 M LiPF<sub>6</sub> in EC:DMC 1 : 1 v/v with 3.3 ppm moisture level, as per the description given by the manufacturer). An appropriate amount of active material was placed in a Teflon bottle at 30°C for 10 days under vacuum, along with the electrolyte solution. The experimental setup is graphically illustrated in Fig. 9. After 10 days, the active material was carefully cleaned and employed for ICP, XRD, surface morphological, and cycling studies. The XRD pattern showed no obvious differences between the before and after aged

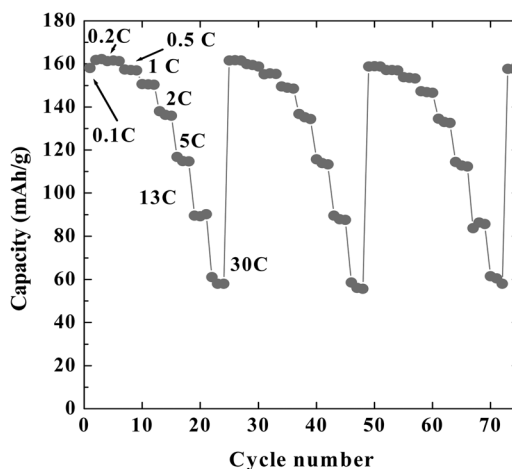


Fig. 8. Rate capability performance of the Li/LiFePO<sub>4</sub> cell at room temperature obtained by a sol-gel route.

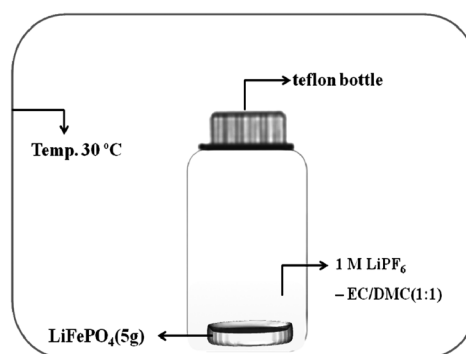


Fig. 9. Pictorial representation of the experimental setup for aging test.

samples (Fig. 10). However, the ICP study revealed dissolution of the Fe<sup>2+</sup> ions in the electrolyte (41.88 ppm before and 35.41 ppm after aged) solution. The 15.45% of the Fe<sup>2+</sup> ions were dissolved in the electrolyte solution. As mentioned earlier, the presence of HF in the electrolyte lead to dissolution of transition metal cations.<sup>26-31)</sup> It proved difficult to detect such dissolution by XRD as it was at a very low concentration for the instrumental standards. The dissolution was obviously seen from the surface morphology of the samples and is given in Fig. 11. From a morphological point of view, the powder-like deposition, along with the active particles, indicated that dissolution occurred during the aging process.

The cycling performance of aged LiFePO<sub>4</sub> was also compared with the pristine material obtained from SS and is given in Fig. 12. The cycling study reveals the

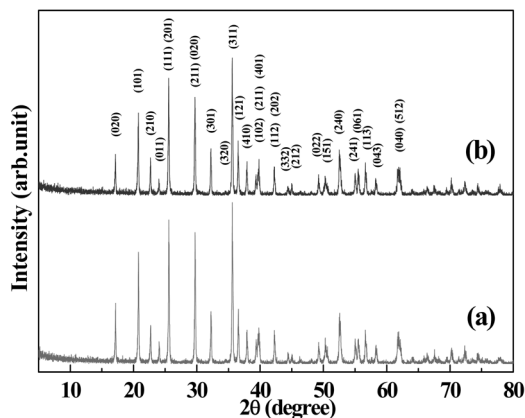


Fig. 10. XRD patterns of LiFePO<sub>4</sub> obtained by the solid-state method (a) before and (b) after aging test.

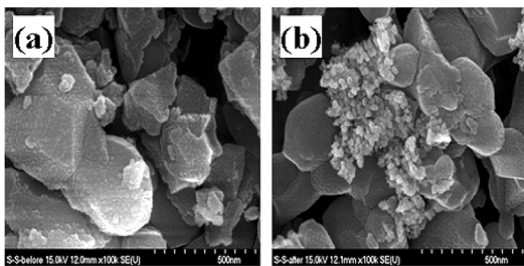


Fig. 11. SEM pictures of LiFePO<sub>4</sub> obtained by the solid-state method (a) before and (b) after aging test.

worse performance of the aged material, showing an initial discharge capacity of 92 mAh/g, which is 71 mAh/g less than the material obtained by the SG route. There are two possible reasons for such performances: (i) Fe<sup>2+</sup> dissolution from LiFePO<sub>4</sub> leads to formation of the amorphous phase under these conditions; (ii) dissolution of Fe<sup>2+</sup> by exchange with H<sup>+</sup> (from HF), which forms the LiH<sub>2</sub>PO<sub>4</sub> phase.<sup>29, 30)</sup> Further, the reaction between LiFePO<sub>4</sub> and HF also leads to formation of the H<sub>3</sub>PO<sub>4</sub> phase; however, it may dissolve in the same organic solutions.<sup>30)</sup> Moreover, the formation and dissolution processes of the H<sub>3</sub>PO<sub>4</sub> phase does not affect the cell, but rather slows down the transport properties of the Li<sup>+</sup> ions. The LiFePO<sub>4</sub> synthesized by the SS method behaves totally different than those synthesized by the SG process, which is in good agreement with the earlier reports by Aurbach *et al.*<sup>30)</sup>

#### 4. Conclusions

To conclude, nanocrystalline LiFePO<sub>4</sub> materials were

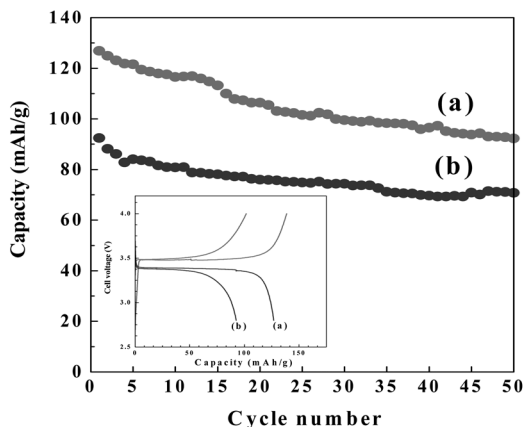


Fig. 12. Cycling performances of LiFePO<sub>4</sub> samples obtained by the solid-state method (a) before and (a) after aging tests. Inset shows the initial charge/discharge curves of the LiFePO<sub>4</sub> samples obtained by the solid-state method (a) before and (b) after aging under room temperature conditions.

synthesized under an Ar atmosphere by solid-state and sol-gel routes at 660 and 670°C, respectively. The Li/LiFePO<sub>4</sub> cell synthesized by the sol-gel method not only offered a high discharge capacity (> 150 mAh/g), it exhibited excellent cycle retention at various current densities from 0.1 to 30 C. The elevated temperature performances of the cells were also demonstrated, with the LiFePO<sub>4</sub> obtained from the sol-gel method showing superior performance than those from the solid-state method. The presence of chelating agent played a crucial role for such improvement of electrochemical performance in the cell. The aging tests were also conducted to corroborate the worse performance of the material synthesized by the solid-state process. Thus, the nanocrystalline LiFePO<sub>4</sub> synthesized by the sol-gel route is a promising candidate for forthcoming lithium batteries.

#### Acknowledgement

The authors gratefully acknowledges the support of “Advanced materials and components project in Gwangju funded by Korea Institute of Industrial Technology (KITECH)”

#### References

1. A.K. Padhi, K.S. Nanjundaswamy and J.B. Goodenough, *J. Electrochem. Soc.*, **144**, 1188 (1997).
2. A. Yamada, S.C. Chung and K. Hinokuma, *J. Electrochem.*

- Soc., **148**, A224 (2001).
3. S.Y. Chung, J.T. Bloking and Y.M. Chiang, *Nat. Mater.*, **1**, 123 (2002).
  4. E.M. Bauer, C. Bellitto, M. Pasquali, P.P. Prosini and G. Righini, *Electrochem. Solid-State Lett.*, **7**, A85 (2004).
  5. A. Manthiram, A.V. Murugan, A. Sarkar and T. Muraliganth, *Energy Environ. Sci.*, **1**, 621 (2008).
  6. R. Dominko, M. Bele, M. Gaberscek, M. Remskar, D. Hanzel, J.M. Goupil, S. Pejovnik and J. Jamnik, *J. Power Sources*, **153**, 274 (2006).
  7. H. Huang, S.C. Yin and L.F. Nazar, *Electrochem. Solid-State Lett.*, **4**, A170 (2001).
  8. S. Yang, Y. Song, P.Y. Zavalij and M.S. Whittingham, *Electrochem. Commun.*, **4**, 239 (2002).
  9. F. Croce, A.D. Epifanio, J. Hassoun, A. Depluta, T. Olczac and B. Scrosati, *Electrochem. Solid-State Lett.*, **5**, A47 (2002).
  10. R. Dominko, J.M. Goupil, M. Bele, M. Gaberseck, M. Remskar, D. Hanzel and J. Jamnik, *J. Electrochem. Soc.*, **152**, A843 (2005).
  11. A.D. Spong, G. Vitins and J.R. Owen, *J. Electrochem. Soc.*, **152**, A2376 (2005).
  12. R. Dominko, M. Bele, M. Gaberscek, M. Remskar, D. Hanzel and S. Pejovnik, *J. Electrochem. Soc.*, **152**, A607 (2005).
  13. P.S. Herle, B. Ellis, N. Coombs and L.F. Nazar, *Nat. Mater.*, **3**, 147 (2004).
  14. P.P. Prosini, M. Lisi, D. Zane and M. Pasquali, *Solid State Ionics*, **148**, 45 (2002).
  15. K.S. Park, J.T. Son, H.T. Chung, S.J. Kim, C.H. Lee and H.G. Kim, *Electrochem. Commun.*, **5**, 839 (2003).
  16. S. Yang, P.Y. Zavalij and M.S. Whittingham, *Electrochem. Commun.*, **3**, 505 (2003).
  17. K. Saravanan, M.V. Reddy, P. Balaya, H. Gong, B.V.R. Chowdari and J.J. Vittal, *J. Mater. Chem.*, **19**, 605 (2009).
  18. G.X. Wang, S. Bewlay, J. Yao, J.H. Ahn, S.X. Dou and H.K. Liu, *Electrochem. Solid-State Lett.*, **7**, A503 (2004).
  19. J. Yang and J.J. Xu, *Electrochemical and Solid-State Lett.*, **7**, A515 (2004).
  20. C.R. Sides, F. Croce, V.Y. Young, C.R. Martin and B. Scrosati, *Electrochem. Solid-State Lett.*, **8**, A484 (2005).
  21. M. Takahashi, S. Tobishima, K. Takei and Y. Sakurai, *J. Power Sources*, **97-98**, 508 (2001).
  22. S.T. Myung, S. Komaba, N. Hirosaki, H. Yashiro and N. Kumagai, *Electrochim. Acta*, **49**, 4213 (2004).
  23. S.S. Zhang, J.L. Allen, K. Xu and T.R. Jow, *J. Power Sources*, **147**, 234 (2005).
  24. A.S. Aricò, P. Bruce, B. Scrosati, J.-M. Tarascon and W. van Schalkwijk, *Nat. Mater.*, **4**, 366 (2005).
  25. Z. Li, D. Zhang and F. Yang, *J. Mater. Sci.*, **44**, 2435 (2009).
  26. M. Schmidt, U. Heider, A. Kuehner, R. Oesten, M. Jungnitz and N. Ignat'ev, P. Sartori, *J. Power Sources*, **97-98**, 557 (2001).
  27. R. Oesten, U. Heider and M. Schmidt, *Solid State Ionics*, **148**, 391 (2002).
  28. J.S. Gnanaraj, M.D. Levi, Y. Gofer, D. Aurbach and M. Schmidt, *J. Electrochem. Soc.*, **150**, A445 (2003).
  29. M. Koltypin, D. Aurbach, L. Nazar and B. Ellis, *Electrochem. Solid-State Lett.*, **10**, A40 (2007).
  30. M. Koltypin, D. Aurbach, L. Nazar and B. Ellis, *J. Power Sources*, **174**, 1241 (2007).
  31. K. Amine, J. Liu and I. Belharouak, *Electrochem. Commun.*, **7**, 669 (2005).
  32. D. Choi and P.N. Kumta, *J. Power Sources*, **163**, 1064 (2007).